

Received 11 December 2023, accepted 28 December 2023, date of publication 3 January 2024,  
date of current version 11 January 2024.

Digital Object Identifier 10.1109/ACCESS.2023.3349371

## RESEARCH ARTICLE

# RIS-Assisted Precoding Spatial Modulation: Optimal Design and Performance Analysis

CHAOWEN LIU<sup>1</sup>, (Member, IEEE), FEI YU<sup>1</sup>,  
ZHENGMIN SHI<sup>1</sup>, (Graduate Student Member, IEEE),  
MENGHAN LIN<sup>2</sup>, (Graduate Student Member, IEEE), CHENXI PANG<sup>1</sup>,  
FASONG WANG<sup>3</sup>, AND JIANKANG ZHANG<sup>4</sup>, (Senior Member, IEEE)

<sup>1</sup>School of Communications and Information Engineering and School of Artificial Intelligence, Xi'an University of Posts and Telecommunications, Xi'an 710121, China

<sup>2</sup>School of Information and Communications Engineering, Xi'an Jiaotong University, Xi'an 710049, China

<sup>3</sup>School of Electrical and Information Engineering, Zhengzhou University, Zhengzhou 450001, China

<sup>4</sup>Department of Computing and Informatics, Bournemouth University, BH12 5BB Poole, U.K.

Corresponding author: Jiankang Zhang (jzhang3@bournemouth.ac.uk)

This work was supported in part by the Key Research and Development Project of Shaanxi Province under Grant 2023-YBGY-272; in part by the National Natural Science Foundation of China under Grant 61901366, Grant 61571401, and Grant U1736107; in part by the National Key Research and Development Program under Grant 2019QY0302; in part by the Engineering and Physical Sciences Research Council Projects under Grant EP/W016605/1 and Grant EP/P003990/1; in part by the European Research Council's Advanced Fellow Grant QuantCom under Grant 789028; in part by the Innovative Talent of Colleges and the University of Henan Province under Grant 18HASTIT021; and in part by the National Natural Science Foundation of Henan Province under Grant 192102210088.

**ABSTRACT** Reconfigurable intelligent surface (RIS) is a vital enabler of paradigm-shifting transmission technologies for next-generation wireless. In this paper, we propose a RIS-assisted transmitter precoding spatial modulation (RIS-PSM), such that the transmission reliability of the PSM-modulated multiple-input multiple-output systems can be remarkably enhanced. To fulfill our novel design, a two-phase decision process (TPDP) based optimization algorithm is propounded, such that the optimal transmitter precoding vector and the RIS reflection matrix can be jointly achieved in terms of closed-form. In addition, we design two receive detection algorithms, namely the optimal co-detection (OCD) and the sub-optimal detached detection, by which the indices of the designated receive antenna and the baseband modulated signal can be reliably detected with different levels of computational complexity. Eventually, the achievable error performance is evaluated analytically for the RIS-PSM proposal with the detection of OCD. Simulation and numerical results are depicted to demonstrate the superiorities of the proposed system, as well as to substantiate the accuracy of the performance analysis.

**INDEX TERMS** Reconfigurable intelligent surface (RIS), precoding spatial modulation, joint transmitter precoding and RIS reflection, receive detection, error performance.

## I. INTRODUCTION

For the past decades, with the number of communication users being dramatically increased, the demand for data traffic has been growing beyond the capacity limit of wireless cellular systems [1], [2], [3], [4]. To address this issue, spatial modulation (SM) has been proposed as a multiple-input multiple-output (MIMO) technology, which combines traditional amplitude and phase modulation (APM) with

antenna index modulation to improve the spectrum efficiency and energy efficiency of communication systems [5], [6], [7], [8].

SM is a highly-effective MIMO technology, which activates only one transmit antenna to emit APM and the antenna index modulation based supersymbols [6], [8], [9], [10]. This kind of SM is also referred to as the transmit SM (TSM), and has attracted widespread research attention in the area of desirable spectral efficiency and energy efficiency trade-off based wireless. As a counterpart to the TSM, linear transmitter precoding empowered receive SM (RSM) is first raised

The associate editor coordinating the review of this manuscript and approving it for publication was Chengpeng Hao<sup>1</sup>.

and investigated in [11], where both the indices of receive antennas and base-band APM symbols are exploited to convey information. Based on the utilization of precoding, the RSM modulated MIMO is capable of attaining both the transmit and receive spatial diversity for accomplishing highly reliable detection of the RSM super-symbols [12], [13]. In [14], the authors have investigated the theoretical performance of the receive antenna shift keying (RASK) scheme by utilizing zero-forcing (ZF) precoding, and have proposed coherent and incoherent detection schemes based on the maximum likelihood (ML) detector. Furthermore, in order to reduce the radio-frequency (RF) front-end complexity of the coherent system, the authors propose to reduce the number of RF chains upon utilizing switches.

Due its advantages in enhancing wireless coverage, reliability, and spectral efficiency of next-generation communications, reconfigurable intelligent surface (RIS), also known as intelligent reflection surface (IRS) or large intelligent surface (LIS), has been recognized as a promising and economical enabling technology for future wireless. The RIS can effectively control the phase, amplitude, frequency, and even polarization of its elements without the need for complex decoding and encoding operations [15], [16], [17]. Specifically, the RIS is equipped with a large number of small, low-cost, and controllable passive components, which can change the reflection coefficient of each element to cancel the phase of the transmitted signal and intelligently reconfigure the wireless communication environment with high flexibility, thereby significantly improving the communication quality of wireless links. The advantages of RIS in technology compatibility, hardware complexity and SM in spectrum resources are combined to achieve further enhanced system performance.

The integration of RIS and SM technology has significantly improved the spectrum and energy efficiency, and hence has attracted widespread attention. In [18], the authors have introduced the RIS into index modulation (IM) field first, and have proposed the RIS-assisted space shift keying and SM scheme. In RIS-IM scheme, the incoming signal is reflected through RIS to improve the system's reception capability, and the IM principle is used to increase the index of multiple antennas, thereby improving spectrum efficiency. In [19], the practical structure combining LIS with SM (LIS-SM) is considered, which can simultaneously utilize transceive antennas indices to achieve higher transmission efficiency. In [20], the RIS-aided receive quadrature SM (RIS-RQSM) was studied, where the IRS elements have been partitioned into two halves to serve the in-phase and the quadrature components separately. Inspired by [20], the authors in [21] have considered both the transmit-end and receive-end using quadrature SM, where the RIS has two panels, each of which assists in directing the real and imaginary parts of the transmitted symbols to the selected receive antennas by adjusting its reflection coefficients. Moreover, the paper has also introduced a low-complexity detection algorithm for the received signal based on compressed

sensing framework, which provided an optimal trade-off between the bit error rate (BER) and complexity. In [22], the authors have investigated the RIS-assisted symbiotic radio system and proposed a scheme with receive antenna index (RAI) modulation characteristics, namely symbiotic SM (SSM) scheme, and conducted theoretical analysis on its detection performance. In [23], the authors have investigated an innovative augmented pattern index modulations (APIM) system enabled by RIS, where the indices of activated patterns of the transmitter, receiver and the RIS are jointly employed for bearing information.

In contrast to the aforementioned references, the concept of precoding is considered in combination with SM, and thus, its undeniable potential can be utilized to enhance the reliability and spectral efficiency of wireless transmission. Specifically, the author of [11] has proposed a transmitter precoding assisted SM (PSM) scheme that transmitted information through joint traditional APM and precoding assisted spatial shift keying modulation for the first time. This scheme is capable of achieving better BER performance than existing schemes when properly designed. The authors of [24] have investigated an generalised precoding aided SM (GPSM) scheme, where the key idea is that a particular subset of receive antennas is activated and the activation pattern itself conveys useful information. Motivated by [24], the authors of [25] have extended the GPSM scheme by incorporating a receive antenna transition pattern, so as to improve the error performance of the generalized precoding-aided SM. In [26], the authors have investigated the TPSM scheme, which can simultaneously achieve transmit and receive diversity. In the TPSM scheme, both transmitter ZF and minimum mean square error precoding have been considered to facilitate low-complexity signal detection. In [27], the authors have proposed to divide the transmit and receive antennas into transceive antennas groups, such that the philosophy of generalized SM is transplanted to a new precoding-assisted massive MIMO system.

Although the modulation framework based on RIS and SM has been extensively studied [18], [19], [20], [21], [22], [23], current researches consider mainly the combination of RIS and SM or that of precoding and SM, which still suffers from high error rates. Meanwhile, it is not feasible to improve the BER performance of RIS-SM system by employing precoding technology straightforwardly. Moreover, in the related research works, transmitter precoding techniques are less reported to be introduced into the multi-antenna transmitter based RIS-RSM for achieving the transceiver and RIS reflection diversity enhancement simultaneously.

Enlightened by the above, in this paper, we propose a novel paradigm for joint RIS reflection and transmitter precoding (JRRTTP) assisted SM, which is named as RIS-assisted precoding SM (RIS-PSM). Subsequently, a two-phase decision process (TPDP) algorithm is designed to derive closed-form optimal RIS reflection coefficients and transmitter precoding vectors. To address varying trade-offs between detection performance and complexity, we introduce two

algorithms: optimal co-detection (OCD) and the sub-optimal detached detection (SODD). Moreover, the discrete-input continuous-output memoryless channel (DCMC) capacity and the average bit error probability (ABEP) performance of the RIS-PSM system are evaluated. Finally, in the simulation analysis, the superiority of the proposed system is demonstrated by comparing it with other spatial domain index modulations (SDIMs). Specific contributions are detailed as follows.

- We propose a RIS enabled spatial domain index modulation scheme, in which the indices of pre-determinate receive antenna and APM modulated baseband symbol are utilized for useful information delivering. In the novel RIS-PSM, based on the JRRTP design, the spatial diversity augmented by RIS-based multi-path reflection can be properly exploited for further significant receiving performance enhancement.
- In order to achieve with the best possible receive performance, an optimization problem of maximizing the useful signal power measured at the designated receive antenna is established for the constructed RIS-PSM system. Due to the non-convexity of the formulated problem, we devise a TPDP algorithm to provide the closed-form suboptimal RIS reflection coefficient and the optimal transmitter precoding solutions respectively.
- We introduce an maximum-likelihood criterion based OCD, such that the joint optimal detection of the pre-specified receive antenna and APM symbol indices can be achieved. Whereas, the complexity of OCD can be unacceptably high for receivers with limited resources. To deal with this, we propose a SODD detector, by which the pre-specified indices are detected separately.
- In order to assess the ceiling of the achievable performance, the DCMC capacity and the ABEP performance of the RIS-PSM systems are analyzed respectively based on the condition that the OCD is utilized. Based on further steps of simplification and approximation, we achieve the spatial diversity order provided by the receiver of the RIS-PSM with a summarizing remark.

The rest of the article is organized as follows. In Section II, we describe the system method of the traditional PSM, and that of the proposed RIS-PSM, while formulate the optimization problem. Section III elaborates the algorithm designed for solving the formulated optimization problem. This is followed by the detection algorithms detailed in Section IV. Section V analyzes the ABEP of the RIS-PSM systems employing with the OCD. Simulation and numerical results are presented in Section VI, whilst our conclusions are summarized in Section VII.

*Notations:* Bold capital letters indicate matrices, while bold lower case letters indicate vectors.  $\mathbb{C}^{m \times n}$  denotes the space of  $(m \times n)$  complex-valued matrices.  $\mathbf{A}_{m \times n}$  represents a matrix of  $m$  rows and  $n$  columns.  $\mathbf{e}_r$  is the  $r$ -th column of the identity matrix.  $j = \sqrt{-1}$  is the imaginary unit.

$(\cdot)^H$  denotes the Hermitian transpose operator.  $\mathbb{E}[\cdot]$  represents the statistical expectation operator.  $\odot$  denotes the Hadamard product.  $\|\cdot\|_p$  represents the  $\ell_p$  norm calculator.  $|\cdot|$  denotes the modular calculator scalar.  $\Re(\cdot)$  derives the real-component(s) of complex scalar or vector.

## II. SYSTEM PROPOSAL AND PROBLEM FORMATION

In this section, we begin with a brief review of the traditional PSM system for completeness. Then, a novel proposal of RIS-PSM is raised, where RIS is employed to provide with multiple spatial propagating paths for transmission performance enhancement. To this point, the advantages of RIS and that of PSM are integrated in one system. In order to accomplish the ideal design of RIS-PSM, we formulate the problem of maximizing the observing signal power over arbitrarily given receive antenna.

### A. CONVENTIONAL PSM SYSTEM

As demonstrated in [11], by contrast to the pure SM, the information bits delivered in each time slot of the PSM system are divided into two portions, where the first portion is referred to the RAI information bits, and the second portion is referred to the conventional  $M$ -ary APM symbol index (ASI) information bits. Based on the mapping of the RAI information bits, the PSM employs a linear transmitter precoding scheme to identify the index of the desired receive antenna  $r$  ( $r \in \{1, 2, \dots, A_R\}$ ), where  $A_R$  denotes the number of antennas equipped with the receiver. Correspondingly, the  $m$ -th ( $m \in \{1, 2, \dots, M\}$ ) symbol can be selected from the  $M$ -ary APM symbol set upon the mapping of the remaining ASI information bits. As both RAI and ASI are utilized to carry information, we can have the total number of information bits conveyed per PSM-modulated superimposed symbol as

$$B = \log_2(A_R) + \log_2(M). \quad (1)$$

For the sake of simplicity, we assume in the context that  $A_R$  and  $M$  are non-negative integer powers of 2.

After the precoding operation, the received signal vector can be expressed as

$$\mathbf{y} = \mathbf{T}\mathbf{s}_m^r + \mathbf{n}, \quad (2)$$

where,  $\mathbf{T}$  is the channel between the transmitter and receiver,  $\mathbf{s}_m^r = \mathbf{P}\mathbf{e}_r x_m$  is the transmitted signal vector,  $\mathbf{P}$  denotes the transmitter precoding matrix,  $x_m$  is the  $m$ -th symbol selected from the APM set with  $\mathbb{E}[|x_m|^2] = 1$ , while  $\mathbf{n}$  is the zero-mean circularly symmetric complex Gaussian noise vector.

Notice that, the conventional PSM system is capable of achieving simultaneously the transmit and receive spatial diversity for BER performance enhancement. Inspired by this, in the following we propose a RIS empowered PSM system with dedicated transmit precoding design, such that the reliability performance of the PSM modulated wireless communication systems can be further reinforced.

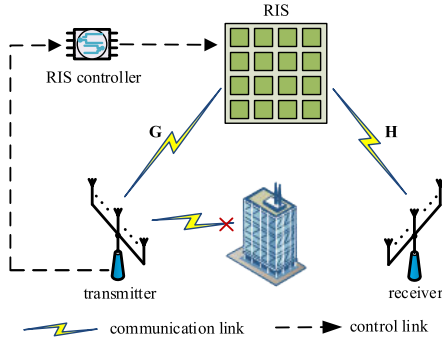


FIGURE 1. System model of the RIS-PSM.

**B. PROPOSED RIS-PSM SYSTEM**

As illustrated in Fig. 1, an RIS-PSM system is considered, in which a RIS with  $A_S$  reconfigurable electronic-magnetic reflection elements is deployed to enhance the quality of transmission from a transmitter with  $A_T$  antennas to a receiver with  $A_R$  antennas. Explicitly, we adopt the assumption that  $A_T$ ,  $A_S$  and  $A_R$  are unexceptionally non-negative integer power of 2, while let  $A_T \geq A_R$  to facilitate the implementation of transmitter precoding. As discussed in many papers, RIS is able to reconfigure the amplitude or phase shift of the reflecting elements, and adjust the reflecting waves to create a specific spatial pattern during each transmission duration [17]. Due to serious path loss, the signals reflected by the RIS two or more times are ignored in this paper, and we assume that the distance between the horizontal and vertical arrays is not less than half of the carrier signal wavelength in RIS.

Let the matrices of the wireless channel between the transmitter and the RIS, and that between the RIS and the receiver can be denoted as  $\mathbf{G} \in \mathbb{C}^{A_S \times A_T}$  and  $\mathbf{H} \in \mathbb{C}^{A_R \times A_S}$ , respectively. In this paper, we consider also the scenario as in [18], [19], and [23], where the transmitter and the receiver is not directly linked due to obstacles, while propose to exploit RIS-assited transmission schemes for enabling reliable wireless transceive connection. Similar to the case in RIS-assisted downlink investigation [28], the complex baseband channel  $\mathbf{H}$  is supposed to obey Rayleigh fading, with each of its elements independently satisfying the complex-Gaussian distribution of  $\mathcal{CN}(0, 1)$ . Moreover, we assume that the channel  $\mathbf{G}$  obeys the Rician fading while letting it be expressed as

$$\mathbf{G} = \sqrt{\frac{K}{K+1}} \mathbf{G}^{\text{LoS}} + \sqrt{\frac{1}{K+1}} \mathbf{G}^{\text{NLoS}}, \quad (3)$$

where,  $K$  is the Rician factor,  $\mathbf{G}^{\text{LoS}}$  and  $\mathbf{G}^{\text{NLoS}}$  denote the deterministic line-of-sight (LoS) component, and the non-LoS (NLoS) component of  $\mathbf{G}$ , respectively. In addition, the NLoS channel of  $\mathbf{G}^{\text{NLoS}}$  is considered to be Rayleigh fading, while the LoS counterpart of  $\mathbf{G}^{\text{LoS}}$  to be the LoS fading. Accordingly,  $\mathbf{G}^{\text{LoS}}$  can be modelled and formulated as

$$\mathbf{G}^{\text{LoS}} = \beta \mathbf{a}_{A_S}(\phi_r) \mathbf{a}_{A_T}^H(\phi_t). \quad (4)$$

Here,  $\beta$  is the path gain,  $\mathbf{a}_{A_S}(\phi_r)$  and  $\mathbf{a}_{A_T}(\phi_t)$  are the steering vectors, which can be given by

$$\mathbf{a}_{A_S}(\phi_r) = [1, e^{j\frac{2\pi d}{\lambda} \sin(\phi_r)}, \dots, e^{j\frac{2\pi d}{\lambda} (A_S-1) \sin(\phi_r)}]^T, \quad (5)$$

$$\mathbf{a}_{A_T}(\phi_t) = [1, e^{j\frac{2\pi d}{\lambda} \sin(\phi_t)}, \dots, e^{j\frac{2\pi d}{\lambda} (A_T-1) \sin(\phi_t)}]^T, \quad (6)$$

in which,  $d$  is the antenna separation distance,  $\lambda$  is the carrier wavelength, while  $\phi_r$  and  $\phi_t$  are the arrival angle at the RIS and the departure angle at the transmitter, respectively. In the context, we simply let  $\frac{d}{\lambda} = \frac{1}{2}$ .

Let the diagonal matrix of RIS reflection coefficients be denoted as  $\Theta = \text{diag}(\theta)$ , where  $\theta = [e^{-j\Phi_1}, e^{-j\Phi_2}, \dots, e^{-j\Phi_{A_S}}]$ ,  $\Phi_l \in (0, 2\pi]$ ,  $l \in \{1, 2, \dots, A_S\}$ . Then, the signal observed vector at the receiver can be written as

$$\mathbf{y} = \sqrt{P_S} \mathbf{H} \Theta \mathbf{G} \mathbf{W} \mathbf{x}_m + \mathbf{z}, \quad (7)$$

where  $P_S$  represents the transmission power,  $\mathbf{W} \in \mathbb{C}^{A_T \times A_R}$  denotes the normalized transmitter precoding matrix.  $\mathbf{x}_m = \mathbf{e}_r x_m$  is the super-symbol, where  $x_m$  is the  $m$ -th symbol in the set of APM symbols ( $m \in \{1, 2, \dots, M\}$ ),  $\mathbf{e}_r \in \mathbb{C}^{A_R \times 1}$  is the activation antenna vector, whose  $r$ -th element is 1 and the rest is 0.  $\mathbf{z} \in \mathbb{C}^{A_R \times 1}$  denotes the complex noise vector, which is composed of complex-Gaussian scalars with zero mean and unit variance.

Similar to the PSM reviewed in Section II-A, in the RIS-PSM, the designated RAI and ASI are selected based on  $\log_2(A_R)$  and  $\log_2(M)$  information bits mapping, and are denoted as  $r$  and  $m$  respectively. As a result, the number of information bits conveyed in each RIS-PSM symbol can be expressed as

$$B = \log_2(A_R) + \log_2(M). \quad (8)$$

**C. PROBLEM FORMATION FOR OPTIMAL DESIGN OF RIS-PSM**

As elaborated in the initiate PSM proposal [11], the linear transmitter precoding of ZF is employed to ensure that the signal observation power of the intended receive antenna for SSK is maximized, while the signal observation power of the left  $(A_R - 1)$  receive antenna(s) is minimized. Similarly, in our novel RIS-PSM, we prepare to achieve the transmitter precoding matrix  $\mathbf{W}$  and RIS reflection coefficient matrix  $\mathbf{H}$ , such that the output signal power is maximized at the specified receive antenna, and nulled at the other  $(A_R - 1)$  receive antenna. To this end, the optimization problem of maximizing the power yielded at the  $r$ -th receive antenna is formulated as follows.

From (7), we can have the signal observed at  $r$ -th receive antenna as

$$y_r = \sqrt{P_S} \mathbf{h}_r \Theta \mathbf{G} \mathbf{W} \mathbf{e}_r x_m + z_r. \quad (9)$$

Let  $\mathbf{w}_r = \mathbf{W} \mathbf{e}_r$ . Then, the reception power of the RIS-PSM modulated super-symbol achieved by the  $r$ -th receive antenna can be expressed as

$$E_{y_r} = P_S |\mathbf{h}_r \Theta \mathbf{G} \mathbf{w}_r|^2. \quad (10)$$

Consequently, we can construct the maximization problem of  $E_{y_r}$  in (10) as

$$P_0 : \max_{\Theta, \mathbf{w}_r} |\mathbf{h}_r \Theta \mathbf{G} \mathbf{w}_r|^2 \quad (11a)$$

$$\text{s.t.} \quad \mathbf{w}_r^H \mathbf{w}_r = P_S \quad (11b)$$

$$\mathbf{w}_r^H (\hat{\mathbf{H}} \Theta \mathbf{G})^H = \mathbf{0}_{1 \times (A_R - 1)} \quad (11c)$$

$$\Theta = \text{diag}[e^{-j\Phi_1}, e^{-j\Phi_2}, \dots, e^{-j\Phi_{A_S}}], \quad (11d)$$

where,  $\hat{\mathbf{H}}$  denotes the channel from the RIS to the other  $(A_R - 1)$  receive antennas, i.e.,  $\hat{\mathbf{H}} = [\mathbf{h}_1^T, \dots, \mathbf{h}_{r-1}^T, \mathbf{h}_{r+1}^T, \dots, \mathbf{h}_{A_R}^T]^T$ ,  $\mathbf{w}_r$  and  $\Theta$  are the optimization variables, (11b) denotes the maximum power constraint of  $\mathbf{w}_r$ , (11c) denotes the ZFC, (11d) denotes the phase constraint of RIS reflection coefficient in  $\Theta$ .

It is worth noting that, in the initial PSM [11], given the channel information, the transmitter precoding matrix is explicitly calculated in integrity. However, in the RIS-PSM, we only need to achieve the transmitter precoding vector  $\mathbf{w}_r$ , upon solving the problem of  $P_0$  once within a channel-invariant duration. Given the same channel, the optimal solution of  $\Theta_r$ , which is also obtained via solving  $P_0$ , differs as  $r$  changes. Hence, we below introduce  $\Theta_r$  for avoiding confusion on understanding  $\Theta$ .

### III. JOINT RIS REFLECTION AND TRANSMITTER PRECODING DESIGN

In this section, we propose the TPDP optimization algorithm to solve the non-convex problem formulated in (11a)-(11d). To begin with, the first phase of TPDP is elaborated in the first half of this section, where a suboptimal but computationally efficient solution of the RIS reflection coefficient matrix is obtained. Following that, we detail the second phase of TPDP, in which the optimal ZFC based transmitter precoding (ZFC-TPC) vector is obtained.

#### A. OPTIMAL DESIGN OF RIS REFLECTION

From (3), it can be indicated that the LoS component  $\mathbf{G}^{\text{LoS}}$  plays a vital role in influencing the quality of channel  $\mathbf{G}$ , especially when  $K \gg 0$ . Besides, given the known position of the transmitter, it is reasonable to place RIS near the transmitter, and treat the connection between them as in a LoS manner [29]. Based on these, it is acceptable for us to ignore the NLoS component of  $\mathbf{G}$ , in order that the closed-form sub-optimal solution of  $\Theta_r$  can be efficiently derived. To do so, we can have  $\tilde{\mathbf{G}}$ , which is the NLoS approximation of  $\mathbf{G}$ , as

$$\tilde{\mathbf{G}} \stackrel{\Delta}{=} \alpha \boldsymbol{\tau} \mathbf{v}^H \approx \beta \mathbf{a}_{A_S}(\phi_r) \mathbf{a}_{A_T}^H(\phi_t), \quad (12)$$

where  $\alpha$  is the path gain factor, while  $\boldsymbol{\tau} \in \mathbb{C}^{A_S}$  and  $\mathbf{v} \in \mathbb{C}^{A_T}$  represent the normalized array response vectors associated with the RIS and the transmitter respectively. From (12), we can achieve that  $\boldsymbol{\tau} \approx \mathbf{a}_{A_S}(\phi_r)$  and  $\mathbf{v} \approx \mathbf{a}_{A_T}(\phi_t)$ . Then, the objective function in  $P_0$  can be approximately re-written as

$$\begin{aligned} |\mathbf{h}_r \Theta \tilde{\mathbf{G}} \mathbf{w}_r|^2 &= |\alpha \mathbf{h}_r \Theta_r \boldsymbol{\tau} \mathbf{v}^H \mathbf{w}_r|^2 \\ &= |\mu \boldsymbol{\theta}_r^T \boldsymbol{\Omega}|^2, \end{aligned} \quad (13)$$

where  $\mu = \mathbf{v}^H \mathbf{w}_r$ ,  $\boldsymbol{\Omega} = \alpha(\mathbf{h}_r \odot \boldsymbol{\tau})$ ,  $\odot$  denotes the Hadamard product. Consequently, we can simplify and reshape  $P_0$  to its suboptimal translation as

$$P_1 : \max_{\Theta_r} |\mu \boldsymbol{\theta}_r^T \boldsymbol{\Omega}|^2 \quad (14a)$$

$$\text{s.t.} \quad (11b), \mathbf{w}_r^H (\hat{\mathbf{H}} \Theta_r \mathbf{G})^H = \mathbf{0}_{1 \times (A_R - 1)} \quad (14b)$$

$$\Theta_r = \text{diag}[e^{-j\Phi_1^r}, e^{-j\Phi_2^r}, \dots, e^{-j\Phi_{A_S}^r}], \quad (14c)$$

By analysing (13), one can be hinted that, in the transformed objective function, the optimization variables,  $\boldsymbol{\theta}_r$  and  $\mathbf{w}_r$  are decoupled, and the maximization of the objective function in  $P_1$  is degenerated to be solved by considering only the adjustment of  $\boldsymbol{\theta}_r$ . To this end, we further transform  $P_1$  to the problem of  $P_2$  as

$$P_2 : \max_{\boldsymbol{\theta}_r} |\boldsymbol{\theta}_r^T \boldsymbol{\Omega}| \quad (15a)$$

$$\text{s.t.} \quad \boldsymbol{\theta}_r = [e^{-j\Phi_1^r}, e^{-j\Phi_2^r}, \dots, e^{-j\Phi_{A_S}^r}]^T, \quad (15b)$$

From (15b), one can observe that in  $\Theta_r$ , only the phase angles of the involved reflection coefficients can be regulated. Hence, by letting  $\Phi_l^{r,o} = \arg(\Omega_l)$ , we can achieve the maximum of the objective function in  $P_2$  as  $\|\boldsymbol{\Omega}\|_1$ .

As a results, the closed-form sub-optimal solution of  $\Theta_r$  can be obtained as

$$\Theta_r^o = \text{diag}[e^{-j\Phi_1^{r,o}}, e^{-j\Phi_2^{r,o}}, \dots, e^{-j\Phi_{A_S}^{r,o}}] \quad (16)$$

#### B. OPTIMAL DESIGN OF TRANSMITTER PRECODING

Given the optimal solution of  $\Theta_r^o$ , we can transform  $P_0$  to the optimization problem for accomplishing the optimal design of  $\mathbf{w}_r$  as

$$P_3 : \max_{\mathbf{w}_r} |(\mathbf{h}_r \Theta_r^o \mathbf{G}) \mathbf{w}_r|^2 \quad (17a)$$

$$\text{s.t.} \quad (11b), \mathbf{w}_r^H (\hat{\mathbf{H}} \Theta_r \mathbf{G})^H = \mathbf{0}_{1 \times (A_R - 1)}, \quad (17b)$$

Let us define the equivalent channel matrix from the transmitter to the receiver as  $\mathbf{F} = (\hat{\mathbf{H}} \Theta_r^o \mathbf{G})^H$ . Then, the singular value decomposition (SVD) on  $\mathbf{F}$  can be executed as

$$\mathbf{F} = [\mathbf{U}_S \mathbf{U}_\perp] [\boldsymbol{\Lambda} \mathbf{0}]^H \mathbf{V}, \quad (18)$$

where  $\mathbf{U}_\perp$  is the null-space matrix that spans the column space of matrix  $\mathbf{F}$ . By introducing an auxiliary vector of  $\mathbf{w}_r$ , we can have  $\mathbf{w}_r = \mathbf{U}_\perp \mathbf{w}'$  which is employed for releasing the ZFC constraint of (17b), as the condition of  $\mathbf{w}_r^H \mathbf{F} = \mathbf{0}_{1 \times (A_R - 1)}$  is always fulfilled. Upon substituting  $\mathbf{w}_r = \mathbf{U}_\perp \mathbf{w}'$  into (17a)-(17b), an unconstrained optimization translation of  $P_3$  can be obtained as follows

$$P_4 : \max_{\mathbf{w}'} \frac{\mathbf{w}'^H \mathbf{U}_\perp^H \mathbf{G}^H \Theta_r^o \mathbf{h}_r^H \mathbf{h}_r \Theta_r^o \mathbf{G} \mathbf{U}_\perp \mathbf{w}'}{\mathbf{w}'^H \mathbf{U}_\perp^H \mathbf{U}_\perp \mathbf{w}'}. \quad (19)$$

Upon observing  $P_4$ , we employ the generalized Rayleigh-Ritz lemma [30], and can achieve that, the optimal solution of  $\mathbf{w}'$  is the eigenvector corresponding to the largest eigenvalue of the matrix  $\boldsymbol{\Pi} = (\mathbf{U}_\perp^H \mathbf{U}_\perp)^{-1} \mathbf{D}$ , where  $\mathbf{D} = (\mathbf{U}_\perp^H \mathbf{G}^H \Theta_r^o \mathbf{h}_r^H \mathbf{h}_r \Theta_r^o \mathbf{G} \mathbf{U}_\perp)$ . Let us define  $\eta(\cdot)$  as the operator

**Algorithm 1**: TPDP Optimization Algorithm

**Input:** The channel matrix  $G$  and  $H$ .

**Output:** The optimal reflection coefficient matrix  $\Theta_r^o$ , and the optimal transmitter precoding vector  $w_r^o$ .

- 1) Calculate  $\Omega = \alpha(h_r \odot \tau)$  and the phase angle of each element of  $\Omega$  as  $\Phi_l^{r,o} = \arg(\Omega_l^{r,o})$ ;
- 2) Return the optimal solution of  $\Theta_r^o$  as

$$\Theta_r^o = \text{diag}[e^{-j\Phi_1^{r,o}}, e^{-j\Phi_2^{r,o}}, \dots, e^{-j\Phi_{A_S}^{r,o}}];$$

- 3) Perform SVD on  $F$  as  $F = [U_S \ U_\perp][\Lambda \ 0]^H V$ ;
- 4) Introduce auxiliary vector  $w'$ , and construct feasible solution to problem P<sub>3</sub> as  $w_r = U_\perp w'$ ;
- 5) Formulate and calculate the matrix of  $\Pi = (U_\perp^H U_\perp)^{-1} (U_\perp^H G^H \Theta_r^{oH} h_r^H h_r \Theta_r^o G U_\perp)$ ;
- 6) Apply the generalized Rayleigh-Ritz theorem, and derive the optimal solution for  $w'$  as  $w' = \eta(\Pi)$ , where  $\eta(\Pi)$  yields the eigenvector corresponding to the maximum eigenvalue of matrix  $\Pi$ ;
- 7) Calculate  $w_r^o = U_\perp \eta(\Pi)$ , and return it as the optimal transmitter precoding vector.

for calculating the eigenvector corresponding to the largest eigenvalue of a given matrix. Then, we can achieve the optimal of  $w_r^o$  as  $w_r^o = U_\perp \eta(\Pi)$ .

Based on the summary of necessary procedures disclosed in Section III-A and III-B, the overall optimization algorithm of TPDP is outlined in Algorithm 1.

Upon the evaluation of the involved mathematical operations, the computational complexity for solving  $\Theta_r^o$  can be given by  $\mathcal{O}(A_S)$ , that for operating SVD by  $\mathcal{O}((A_R - 1)A_T^2)$ , and that for solving  $w_r^o$  by  $\mathcal{O}(2(A_T - 1)A_T A_S + 2(A_T - 1)A_S^2 + 2(A_T - 1)A_S + (A_T - 1)^2 A_T + (A_T - 1)^5 A_T + 2(A_T - 1)^3)$  [31]. Consequently, the overall computational complexity of the TPDP algorithm can be given by  $\mathcal{O}(A_T^2 A_R + 2A_T^2 A_S + 2A_T A_S^2 + A_T^6 + 10A_T^4 - 2A_S^2 - A_S - 5A_T^5 - 7A_T^3 - 4A_T^2 - 6A_T - 2)$ .

*Remark 1:* As declared above, the sub-optimal RIS reflection coefficient is achieved by leveraging only the NLoS of channel  $\mathbf{G}$ , while the optimal of the transmitter precoding is derived upon employing the sub-optimal of  $\Theta_r^o$  attained. Due to this, the phase-offsets of the RIS-involved cascaded channel elements can not be compensated completely, and the channel phase errors are yielded inevitably. Consequently, the constellation observations achievable by the receiver are randomly distributed in an annulus, while the reliability performance of receiver detection is foreseeably deteriorated to an undesirable situation. Fortunately, the channel phase-errors can be accurately calculated with the ideal CSI acquired, and can be eliminated by multiplying a compensation factor to the transmitting signal. Let  $\mu_r = e^{-\arg(h_r \Theta_r^o \mathbf{G} w_r^o)}$  be the compensation factor corresponding to the  $r$ -th designated receive antenna, we can have the receive signal observation without channel phase errors as

$$\mathbf{y} = \sqrt{P_S} \mathbf{H} \Theta_r^o \mathbf{G} w_r^o \mu_r x_m + \mathbf{z}. \quad (20)$$

*Remark 2:* Based on the investigation of Algorithm 1, we conjecture that the proposed RIS-PSM would be witnessed with BER performance loss when compared with selected SDIM scheme(s), regardless of whether the OCD or SODD algorithm is used for received signal detection, as the optimal precoding vector  $w_r^o$  is obtained based on utilizing the suboptimal RIS reflection coefficient solution of  $\Theta_r^o$ . However, most of the RIS-assisted SDIM schemes can be categorized as receive-side SDIMs, and are generally applicable to uplink MIMOs with only receive and RIS end spatial diversity being available. By contrast, the RIS-PSM proposed in this paper can be applicable to downlink MIMOs, where the transmit, receive and RIS end spatial diversity can be simultaneously obtained for BER performance enhancement. Hence, given the same data rate, the BER performance achievable by the proposed RIS-PSM can surpass that by many other SDIMs by explicitly equipping the transmitter with relatively large number of transmit antennas. These discussion can be exemplified and substantiated in the forthcoming Section of simulations.

**IV. RECEIVING SIGNAL DETECTION**

In this section, we begin with the elaboration of the OCD detector, which is able to achieve the optimal detection with extremely high computational complexity. Then, SODD detector is proposed to tackle different design trade-offs between detection reliability and complexity.

**A. OPTIMAL CO-DETECTION**

To achieve the ideal performance of detection, we introduce the ML estimation based OCD detector to estimate the RAI and ASI jointly. The ML estimation is a probability-based parameter estimation method. Its core idea is to determinate the unknown parameters of the given probability model by maximizing the likelihood function of the sample data [32].

Based on the ML principle, the OCD is proposed to be capable of selecting a PSM-modulated superimposed symbol that maximizes the probability of observing the sample data among all possible superimposed symbols as the detection result. In other words, prior probability information and sample data need to be used to calculate the posterior probability of each possible superimposed symbols through the Bayes formula [32], and the superimposed symbol with the maximum posterior probability is selected as the detection result.

With the OCD detector, the designated RAI  $\hat{r}$  and the ASI  $\hat{m}$  can be obtained by solving the optimization problem formulated as follows

$$\begin{aligned} \langle \hat{r}, \hat{m} \rangle &= \arg \max_{r \in \mathcal{R}, m \in \mathcal{M}} f(\mathbf{y} | \mathbf{H}, \mathbf{G}_r, \mathbf{x}_m) \\ &= \arg \min_{r \in \mathcal{R}, m \in \mathcal{M}} \|\mathbf{y} - \sqrt{P_S} \mathbf{H} \Theta_r^o \mathbf{G} w_r^o \mu_r x_m\|^2, \end{aligned} \quad (21)$$

where,  $f(\mathbf{y} | \mathbf{G}_r, \mathbf{x}_m, \mathbf{H}, \mathbf{W}) = \pi^{-A_R} \exp(-\|\mathbf{y} - \sqrt{P_S} \mathbf{H} \Theta_r^o \mathbf{G} w_r^o \mu_r x_m\|^2)$  is the PDF of the received signal conditioned

on  $\mathbf{G}_r$ ,  $\mathbf{x}_m$ ,  $\mathbf{H}$ , and  $\mathbf{W}$ .  $\mathcal{R} \triangleq \{1, 2, \dots, A_R\}$ , and  $\mathcal{M} \triangleq \{1, 2, \dots, M\}$ .

From (21), we can learn that the OCD requires the RAI and ASI to be searched jointly for each receive antenna. Hence, the computational complexity of OCD is undesirably high. Nevertheless, the situation can be even worse when the numbers of transmit and receive antennas become large.

### B. SUB-OPTIMAL DETACHED DETECTION

To decrease the computational complexity and power consumption at receiver, we follow the principle of noncoherent detection, and propose a novel detecting algorithm of SODD, by which the RAI and ASI are determined at two continuous steps respectively. Specifically, in the first step, the signal power attainable by each receive antenna is measured and sorted. Based on which, we can estimate the RAI via solving

$$\hat{r} = \arg \max_{r \in \mathcal{R}} |y_r|^2. \quad (22)$$

Then, assuming that  $\hat{r}$  has been correctly detected, the signal received by the  $\hat{r}$ -th receive antenna can be represented as

$$y_{\hat{r}} = \sqrt{P_S} \mathbf{h}_{\hat{r}} \mathbf{\Theta}_{\hat{r}}^o \mathbf{G} \mathbf{w}_{\hat{r}}^o \mu_{\hat{r}} x_m + z_{\hat{r}}. \quad (23)$$

Straightforwardly, one can determinate the ASI by utilizing the coherent detector, which is represented as

$$\hat{m} = \arg \min_{m \in \mathcal{M}} |y_{\hat{r}} - \sqrt{P_S} \mathbf{h}_{\hat{r}} \mathbf{\Theta}_{\hat{r}}^o \mathbf{G} \mathbf{w}_{\hat{r}}^o \mu_{\hat{r}} x_m|^2. \quad (24)$$

However, it can be indicated from (24) that, the system complexity for achieving the reliable detection of ASI can be still high, as the complete CSI, as well as optimal transmit perturbation and RIS reflection are requested for accomplishing the detection. From this perspective, the coherent detector formulated by (24) can not be employed by the receiver with limited signal processing resources, while can even be ineffective for the case that only the statistical CSI is available at the receiver. To cope with this, we take further steps on deriving the distribution of  $\Xi = \sqrt{P_S} \mathbf{h}_{\hat{r}} \mathbf{\Theta}_{\hat{r}}^o \mathbf{G} \mathbf{w}_{\hat{r}}^o \mu_{\hat{r}}$ . After that, we complete the elaboration of the proposed SODD with the second detecting step, namely the detection of ASI being updated as

$$\hat{m} = \arg \min_{m \in \mathcal{M}} \left| \frac{y_{\hat{r}}}{\mathbb{E}_{\mathbf{h}_r, \mathbf{G}}[\Xi]} - x_m \right|^2, \quad (25)$$

Since  $\mathbf{\Theta}_{\hat{r}}^o$  and  $\mathbf{w}_{\hat{r}}^o$  is only achievable by utilizing the instantaneous CSIs of  $\mathbf{H}$  and  $\mathbf{G}$ , we cannot directly obtain the distribution of  $\Xi$  with the statistical distributions of the channels  $\mathbf{H}$  and  $\mathbf{G}$ . However, upon adopting the Monte-Carlo simulation based distribution fitting, we find that  $\Xi$  approximately obeys the kernel normal with the distribution parameters to be closely related with the system configuration parameters, like the configuration parameters of transceiving and reflecting arrays. Based on this, we can obtain the mean of  $\Xi$  under specific parameters, as shown

in Table 1. In the subsequent simulations, we will directly adopt data exemplified in Table 1 for symbol detection.

Based on the analysis of (21), it can be determined that the complexity of OCD is  $\mathcal{O}(M A_R A_S A_T^3)$ . Upon analysing the (22) and (25), we can drive that the complexity of SODD is  $\mathcal{O}(A_R A_S A_T^3 + M)$ . From the above analysis, it can be seen that the computational complexity of SODD is lower than that of OCD.

TABLE 1. Mean of  $\Xi$  with system configuration by the kernel normal distribution.

System Configuration			Mean
$A_T$	$A_R$	$A_S$	$\Xi$
2	2	32	14.6
2	2	64	29.1
4	2	32	26.36
4	2	64	52.6
4	4	64	19.38

TABLE 2. Computational complexity comparison of OCD and SODD detectors for RIS-PSM.

Detector	Complexity
RIS-PSM(OCD)	$\mathcal{O}(M A_R A_S A_T^3)$
RIS-PSM(SODD)	$\mathcal{O}(A_R A_S A_T^3 + M)$

### V. PERFORMANCE ANALYSIS OF RIS-PSM SYSTEMS

In this section, we derive the achievable performance results of the proposed RIS-PSM system with OCD detector. To be more specific, we analyze the capacity performance, error performance, and the diversity gain of the investigated RIS-PSM system.

#### A. ANALYSIS OF ACHIEVABLE DCMC CAPACITY

To begin with, we analyse the capacity performance of the RIS-PSM modulated MIMO system with the OCD detector. Unlike Shannon's channel capacity and its derivatives, the channel capacity of RIS-PSM modulated MIMO is evaluated under the condition that the input signal is composed of finite alphabet APM symbols and discrete antenna index symbols. In this sense, the capacity of the RIS-PSM is attained over. The DCMC capacity of the RIS-PSM system can be represented as

$$\begin{aligned} C &= B - 2^{-B} \\ &\times \sum_{r,m} \mathbb{E}_{\mathbf{H}, \mathbf{G}, \mathbf{z}} \left[ \log \sum_{\hat{r}, \hat{m}} \exp\left( \frac{-\|\mathbf{y}_m^r - \mathbf{y}_{\hat{m}}^{\hat{r}} + \mathbf{z}\|^2 + \|\mathbf{z}\|^2}{N_0} \right) \right] \\ &= B - \frac{A_R}{\ln 2} - 2^{-B} \\ &\times \sum_{r,m} \mathbb{E}_{\mathbf{H}, \mathbf{G}, \mathbf{z}} \left[ \log \sum_{\hat{r}, \hat{m}} \exp\left( \frac{-\|\mathbf{y}_m^r - \mathbf{y}_{\hat{m}}^{\hat{r}} + \mathbf{z}\|^2}{N_0} \right) \right], \quad (26) \end{aligned}$$

Then, by referring to the method in [33], we invoke Jensen's inequality and apply it to the logarithmic function  $\log_2(x)$ , a tight approximate expression for the DCMC capacity can

be obtained as

$$C_{AP} = B - 2^{-B} \sum_{r,m} \log \sum_{\hat{r},\hat{m}} \mathbb{E}_{\mathbf{H},\mathbf{G}}[\exp(-\frac{\xi}{2N_0})] \\ = B - 2^{-B} \sum_{r,m} \log \sum_{\hat{r},\hat{m}} M_{\xi}(-\frac{1}{2N_0}), \quad (27)$$

where,  $\xi = \vartheta^2$  and  $\vartheta = \|\mathbf{y}_m^r - \mathbf{y}_{\hat{m}}^{\hat{r}}\|$ , while  $M_{\xi}(\cdot)$  is the moment generating function (MGF) with respect to variable  $\xi$ , which can be defined as [32]

$$M_Z(t) = \mathbb{E}_Z[e^{tZ}] = \int_{-\infty}^{+\infty} \exp(tZ)f(Z)dZ. \quad (28)$$

where  $f(Z)$  is the probability density function (PDF) of the random variable  $Z$ .

It's worth noting that, upon utilizing Monte-Carlo based distribution fitting, we have  $\Xi = \sqrt{P_S} \mathbf{h}_{\hat{r}}^o \mathbf{\Theta}_{\hat{r}}^o \mathbf{G} \mathbf{w}_{\hat{r}}^o \mu_{\hat{r}} x_m$  formulated in Section IV-B approximately obeys the kernel normal distribution. The fitting results of the kernel normal distribution is demonstrated in Fig. 2. Apart from the introduced approximation errors, the exact PDF of kernel distribution is currently difficult to be achieved. Unfortunately, both  $\mathbf{y}_m^r$  and  $\mathbf{y}_{\hat{m}}^{\hat{r}}$  share the common representation form similar to  $\Xi$ , and hence we are not able to deduce feasible solution from (31). Consequently, we continue to evaluate the BER performance, and derive the spatial diversity order achievable by our proposed RIS-PSM, whileleft further simplification of the MGF defined in the context for future consideration.

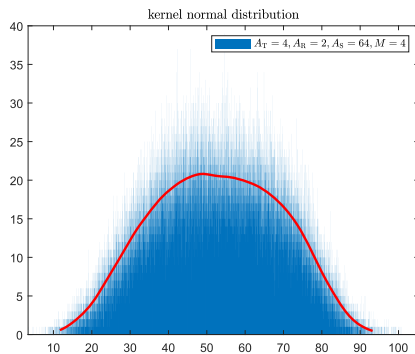


FIGURE 2. The fitting results of the kernel normal distribution.

### B. ANALYSIS OF ACHIEVABLE BIT ERROR RATE

In this subsection, we analyze the BER performance of the proposed RIS-PSM system from the perspective of ABEP. The ABEP of the RIS-PSM system that uses OCD is derived, which characterizes the upper bound of BER performance for RIS-PSM systems with other detections. The ABEP achievable by the RIS-PSM employing with the detector of OCD can be expressed as [8]

$$\bar{P}_e = \frac{1}{B \times 2^B} \mathbb{E}_{\mathbf{H},\mathbf{G}}[\sum_{r,m} \sum_{\hat{r},\hat{m}} D_H(\mathbf{y}_m^r, \mathbf{y}_{\hat{m}}^{\hat{r}}) P\{\mathbf{y}_m^r, \mathbf{y}_{\hat{m}}^{\hat{r}}\}], \quad (29)$$

where,  $D_H(\mathbf{y}_m^r, \mathbf{y}_{\hat{m}}^{\hat{r}})$  denotes the Hamming distance between different symbols,  $P\{\mathbf{y}_m^r, \mathbf{y}_{\hat{m}}^{\hat{r}}\}$  is the conditional probability of the pairwise error event that the RIS-PSM signal  $\mathbf{y}_m^r = \sqrt{P_S} \mathbf{H} \mathbf{\Theta}_r^o \mathbf{G} \mathbf{w}_r^o \mu_r x_m$  is transmitted, whilst  $\mathbf{y}_{\hat{m}}^{\hat{r}} = \sqrt{P_S} \mathbf{H} \mathbf{\Theta}_{\hat{r}}^o \mathbf{G} \mathbf{w}_{\hat{r}}^o \mu_{\hat{r}} x_{\hat{m}}$  is eventually detected.

Given the definition in (29), the conditional pairwise error probability (PEP) can be formulated as

$$P\{\mathbf{y}_m^r, \mathbf{y}_{\hat{m}}^{\hat{r}}\} = \Pr(\|\mathbf{y} - \mathbf{y}_m^r\|^2 > \|\mathbf{y} - \mathbf{y}_{\hat{m}}^{\hat{r}}\|^2), \quad (30)$$

where  $\Pr(\cdot)$  is the statistical calculator. After algebraic manipulation, the conditional PEP can be further deduced as follows

$$P\{\mathbf{y}_m^r, \mathbf{y}_{\hat{m}}^{\hat{r}}\} \\ = \Pr(|\sqrt{P_S} \mathbf{H} \mathbf{\Theta}_r^o \mathbf{G} \mathbf{w}_r^o \mu_r x_m|^2 - |\sqrt{P_S} \mathbf{H} \mathbf{\Theta}_{\hat{r}}^o \mathbf{G} \mathbf{w}_{\hat{r}}^o \mu_{\hat{r}} x_{\hat{m}}|^2 \\ - 2\Re\{\sqrt{P_S} \mathbf{y} (\mathbf{H} \mathbf{\Theta}_r^o \mathbf{G} \mathbf{w}_r^o \mu_r x_m - \mathbf{H} \mathbf{\Theta}_{\hat{r}}^o \mathbf{G} \mathbf{w}_{\hat{r}}^o \mu_{\hat{r}} x_{\hat{m}})\} > 0) \\ = \sqrt{P_S} \Pr(-|\mathbf{H} \mathbf{\Theta}_r^o \mathbf{G} \mathbf{w}_r^o \mu_r x_m - \mathbf{H} \mathbf{\Theta}_{\hat{r}}^o \mathbf{G} \mathbf{w}_{\hat{r}}^o \mu_{\hat{r}} x_{\hat{m}}|^2 \\ - 2\Re\{(\mathbf{H} \mathbf{\Theta}_r^o \mathbf{G} \mathbf{w}_r^o \mu_r x_m - \mathbf{H} \mathbf{\Theta}_{\hat{r}}^o \mathbf{G} \mathbf{w}_{\hat{r}}^o \mu_{\hat{r}} x_{\hat{m}}) \mathbf{z}\} > 0). \quad (31)$$

By bring in the Gaussian Q function, which is defined as  $Q(x) = \frac{1}{\sqrt{2\pi}} \int_x^\infty \exp(-\frac{t^2}{2}) dt$ , we can obtain the simplified expression of the conditional PEP as

$$P\{\mathbf{y}_m^r, \mathbf{y}_{\hat{m}}^{\hat{r}}\} = \Pr(\|\mathbf{y} - \mathbf{y}_m^r\|^2 > \|\mathbf{y} - \mathbf{y}_{\hat{m}}^{\hat{r}}\|^2) \\ = Q(\sqrt{\frac{\|\mathbf{y}_m^r - \mathbf{y}_{\hat{m}}^{\hat{r}}\|^2}{2N_0}}) = Q(\sqrt{\frac{\xi}{2N_0}}). \quad (32)$$

Then, by employing the Jensens inequality, the ABEP union-bound (ABEP-UB)<sup>1</sup> [34] can be achieved as

$$P_{UB} = \frac{1}{B \times 2^B} \sum_{r,m} \sum_{\hat{r},\hat{m}} D_H(\mathbf{y}_m^r, \mathbf{y}_{\hat{m}}^{\hat{r}}) \bar{P}, \quad (33)$$

where  $\bar{P} = \mathbb{E}_{\mathbf{H},\mathbf{G}}[P\{\mathbf{y}_m^r, \mathbf{y}_{\hat{m}}^{\hat{r}}\}]$  is the unconditional PEP. Owing to the involvement of several complex integrals in the expression of unconditional PEP, it is not possible to directly derive a closed-form expression for it, further simplifying the expression of ABEP-UB becomes also difficult. Fortunately, given a sufficiently large number of RIS elements, we adopt the analysis method based on the central limit theorem (CLT) and MGF, such that an approximate upper bound for the ABEP-UB can be obtained.

Upon leveraging the integral definition of the Q function, the unconditional PEP can be written as follows

$$\bar{P} = \int_0^\infty Q(\sqrt{\frac{\xi}{2N_0}}) f_{\xi}(\xi) d\xi \\ = \int_0^\infty \frac{1}{\pi} \int_0^{2/\pi} \exp(\frac{-\xi}{4\sin^2 \varphi N_0}) f_{\xi}(\xi) d\varphi d\xi \\ = \frac{1}{\pi} \int_0^{2/\pi} M_{\xi}(\frac{-1}{4\sin^2 \varphi N_0}) d\varphi, \quad (34)$$

<sup>1</sup>Union-Bound is a classical analysis approach, which can be exploited to calculate an upper bound for the ABEP by summing the probabilities of different error events [34]. This approach indeed provides the tightest upper limit as it takes into account all possible error events of receiver detection.

where  $M_\xi(\cdot)$  can be derived by considering the integral of the exponential function of a Gaussian random variable with general quadratic form. However, apart from the complication of deriving the exact closed-form MGF expression, the definite integral of the intricate MGF with respect to  $\varphi$  can be very difficult to be deduced. Then, to cope with this, we invoke a tight upper bound of the Gaussian Q function [35], and formulate the upper bound of the conditional PEP as

$$P\{\mathbf{y}_m^r, \hat{\mathbf{y}}_{\hat{m}}^r\} \leq \sum_{n=1}^2 \delta_n \exp\left(\frac{-\xi}{\rho_n N_0}\right), \quad (35)$$

where  $\delta = [\frac{1}{12}, \frac{1}{4}]$ ,  $\rho = [\frac{1}{4}, \frac{1}{3}]$ . Therefore, the unconditional PEP can be rewritten as

$$\bar{P} \leq \mathbb{E}_{\mathbf{H}, \mathbf{G}} \left[ \sum_{n=1}^2 \delta_n \exp\left(\frac{-\xi}{\rho_n N_0}\right) \right] = \sum_{n=1}^2 \delta_n M_\xi\left(\frac{-1}{\rho_n N_0}\right), \quad (36)$$

By substituting the unconditional PEP upper bound in (36) into (29), we can achieve that the ABEP-UB is upper-bounded as  $\bar{P}_{\text{UB}} \leq \bar{P}_{\text{UPB}}$ , where the ABEP upper-bound (ABEP-UPB)  $\bar{P}_{\text{UPB}}$  is given by

$$\bar{P}_{\text{UPB}} = \frac{1}{B \times 2^B} \sum_{r,m} \sum_{\hat{r}, \hat{m}} D_{\mathbf{H}}(\mathbf{y}_m^r, \hat{\mathbf{y}}_{\hat{m}}^r) \sum_{n=1}^2 \delta_n M_\xi\left(\frac{-1}{\rho_n N_0}\right). \quad (37)$$

### C. EVALUATION OF ACHIEVABLE SPATIAL DIVERSITY

From (37), it can be observed that the statistical expectation of the random variable  $\xi$  needs to be further simplified, so as to derive the closed-form DCMC capacity and ABEP-UPB for accomplishing the achievable performance evaluation of the RIS-PSM system. Since the transmitter precoding included signal processing is undesirably complicated, it is difficult to explicitly obtain a closed-form result of the statistical expectation of variable  $\xi$ . Therefore, we consider shifting the problem to the derivation of the PDF of  $\xi$ . However, due to the intricate and coupled structure of  $\xi$ , it remains challenging to obtain the accurate PDF of  $\xi$ . Hence, we consider in this subsection to simplify (37) in order to obtain insightful observations regarding the diversity gain, which is achievable by the proposed RIS-PSM.

*Proposition 1:* The statistical expectation represented in (36) can be simplified as

$$\mathbb{E}_{\mathbf{H}, \mathbf{G}} \left[ \exp\left(\frac{-\xi}{\rho_n N_0}\right) \right] = \mathbb{E}_{\mathbf{G}} \left[ \exp\left(-\frac{\rho_n N_0}{\|\boldsymbol{\omega}\|^2 + \rho_n N_0}\right)^{A_R} \right], \quad (38)$$

where, by definition,  $\boldsymbol{\omega} = \boldsymbol{\Theta}_r^o \mathbf{G} \mathbf{w}_r^o \mu_r x_m - \boldsymbol{\Theta}_{\hat{r}}^o \mathbf{G} \mathbf{w}_{\hat{r}}^o \mu_{\hat{r}} x_{\hat{m}}$ .

*Proof:* Recalling (21) and (36), and that  $\vartheta = \|\mathbf{y}_m^r - \hat{\mathbf{y}}_{\hat{m}}^r\|$ , the random variable of  $\xi = \vartheta^2$  can be rewritten as

$$\begin{aligned} \xi &= \|\mathbf{H} \boldsymbol{\Theta}_r^o \mathbf{G} \mathbf{w}_r^o \mu_r x_m - \mathbf{H} \boldsymbol{\Theta}_{\hat{r}}^o \mathbf{G} \mathbf{w}_{\hat{r}}^o \mu_{\hat{r}} x_{\hat{m}}\|^2 \\ &= \|\mathbf{H} (\boldsymbol{\Theta}_r^o \mathbf{G} \mathbf{w}_r^o \mu_r x_m - \boldsymbol{\Theta}_{\hat{r}}^o \mathbf{G} \mathbf{w}_{\hat{r}}^o \mu_{\hat{r}} x_{\hat{m}})\|^2 \\ &= \|\mathbf{H}^H \boldsymbol{\omega}\|^2 \end{aligned} \quad (39)$$

Upon substituting (39) into (36), while invoking the assumption of independent channel fading and introducing the MGF, we can have

$$\begin{aligned} \mathbb{E}_{\mathbf{G}, \mathbf{H}} \left[ \exp\left(\frac{-\xi}{\rho_n N_0}\right) \right] &= \mathbb{E}_{\mathbf{G}, \mathbf{H}} \left[ \exp\left(-\frac{\|\mathbf{H}^H \boldsymbol{\omega}\|^2}{\rho_n N_0}\right) \right] \\ &\stackrel{(a)}{=} \mathbb{E}_{\mathbf{G}} \left[ \left( \frac{\rho_n N_0}{\|\boldsymbol{\omega}\|^2 + \rho_n N_0} \right)^{A_R} \right], \end{aligned} \quad (40)$$

where, the equality of (a) is obtain by leveraging the independence between  $\mathbf{H}$  and  $\boldsymbol{\omega}$ , and the approach of MGF in [34]. ■

*Remark 3:* In the high signal-to-noise ratio (SNR) region of  $\gamma = \frac{1}{N_0} \rightarrow \infty$ , i.e.,  $N_0 \rightarrow 0$ , the result in (38) can be further simplified as

$$\mathbb{E}_{\mathbf{G}, \mathbf{H}} \left[ \exp\left(\frac{-\xi}{\rho_n N_0}\right) \right] = \gamma^{-A_R} \times \mathbb{E}_{\mathbf{G}} \left[ \left( \frac{\rho_n^{A_R}}{\|\boldsymbol{\omega}\|^{2A_R}} \right) \right], \quad (41)$$

From [36], we can learn that, if the average BER of the RIS-PSM system can be expressed as follows

$$\bar{P}_{\text{be}} = c \bar{\gamma}^{-D}, \quad (42)$$

where  $c$  is a constant that depends on the specific modulation and encoding scheme, while  $\gamma$  defines the average received SNR. Then,  $D$  denotes the diversity order of the system. Therefore, upon substituting (41) into (29), we can be implied that the proposed RIS-PSM is able to attain  $A_R$  orders of receive diversity with the employment of  $A_R$  receive antennas.<sup>2</sup>

### VI. SIMULATION RESULTS

In this section, we will characterize and compare the numerical and approximate DCMC capacity performance of the RIS-PSM systems with the detection of OCD. The simulated BER results will be depicted to demonstrate the performance discrepancy of the RIS-PSM systems with the detections of OCD and SODD respectively. Further, we will substantiate the simplified ABEP-UB and ABEP-UPB via Monte-Carlo simulations. In addition, the three-dimensional constellation and BER performance achievable by the RIS-PSM employing with different transmitter precoding schemes will be displayed and compared. Moreover, we compare the BER performance of the proposed RIS-PSM and that of the other three SDIM counterparts [11], [18], [19]. Given the practical consideration of channel estimation, the BER performance attainable by the OCD and SODD based RIS-PSM systems are contradistinguished with different levels of channel estimation errors. Note that, unless otherwise specified in the figures, the simulated system is generally configured with the parameters in Table 3.

Fig. 3 demonstrates the simulated results of the achievable DCMC capacity and the numerical results of its approximation for the RIS-PSM system with the detector of OCD. As can be observed from Fig. 3, both the DCMC capacity

<sup>2</sup>The term of  $\gamma^{-A_R}$  in (41) explains this, when following the definition of diversity order summarized in [36].

TABLE 3. Simulation parameters.

Parameters	Value
Path gains $\alpha, \beta$	1, 1
The number of transmit antennas $A_T$	2
The number of receive antennas $A_R$	2
The number of RIS reflection elements $A_S$	64
Modulation order of APM symbol $M$	4
Rician factor $K$	1

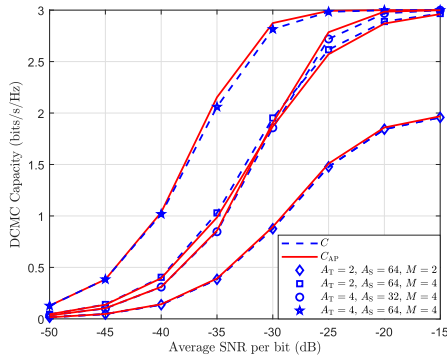


FIGURE 3. Comparison of the DCMC capacity and its approximation achievable by RIS-PSM systems with the OCD.

and its approximate results exhibit logarithmic growth in the low SNR region, increase gradually to their upper limit in the high SNR region. Given the fix configuration of  $A_R = 2$ , the growth rate of the DCMC capacity and its approximation becomes faster as the number of RIS elements  $A_S$  is increased from 32 to 64. For example, in the medium of the SNR range examined, the capacity performance of the proposed system can achieve an approximate SNR gain of more than 5 dB, when letting  $A_S$  be increased from 32 to 64. On the other hand, the growth rate of the capacity performance reveal out to be faster as the number of transmit antennas increases from 2 to 4 which is exemplified with a SNR gain of about 5 dB witnessed in the medium of the SNR range. It can also be seen from the Fig. 3 that, among the considered system configurations, the result of approximate DCMC capacity is closely related to that of the DCMC capacity, which indicates that the simplification of the formula can facilitate us to achieve more insights regarding the performance advantages of the proposed RIS-PSM.

Fig. 4 characterizes the BER performance results of the proposed RIS-PSM systems employing either the detection of OCD or that of SODD, when different system configurations are considered. From Fig. 4, it can be observed that, whether the OCD or SODD is employed by the proposed system, the optimal BER performance is achieved when letting  $A_T = 4$ ,  $A_R = 2$ ,  $A_S = 64$ ,  $M = 4$ . The RIS-PSM system with the detection of OCD is generally capable of achieving better BER performance than its SODD based counterpart, while the BER performance gap between them becomes insignificant, as the number of RIS elements  $A_S$  increases from 32 to 64. Moreover, by observing individual cases of

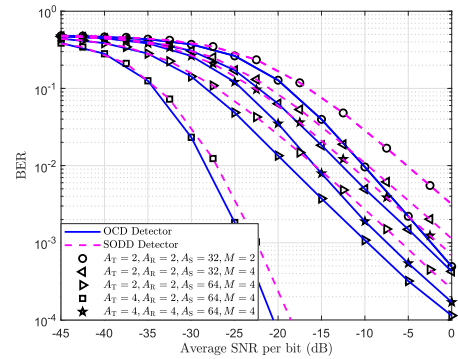


FIGURE 4. Compare of the BER performance achievable by the RIS-PSM systems employing with the detections of OCD and SODD respectively.

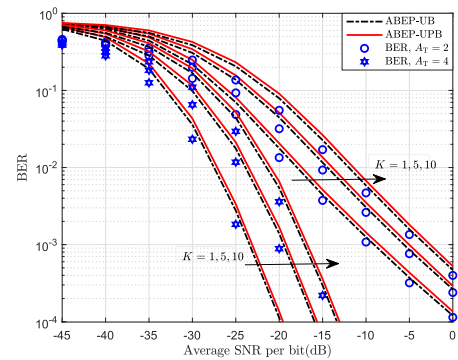


FIGURE 5. Comparison of the simulated BER and numerical ABEP result of the OCD based the RIS-PSM system with different Rician factors.

the proposed system with different detections, we can see that the achievable BER performance is further enhanced as  $A_S$  increases, while deteriorating as  $A_R$  increases. Specifically, when the number of receive antennas  $A_R$  increases from 2 to 4, the system with  $A_R = 4$  requires at least 17 dB of additional SNR to achieve the same BER of  $10^{-3}$  as that with  $A_R = 2$ . This is explicitly due to that the attainable spatial diversity gain is improved when  $A_S$  increases from 32 to 64, while degraded when  $A_R$  increases from 2 to 4.

Fig. 5 depicts the simulated results of the BER, and the numerical results of the ABEP-UB and ABEP-UPB attainable with different Rician factors. From Fig. 5, we can explicitly observe that, the performance results of the ABEP-UB and ABEP-UPB are generally tight, when comparing with the simulate BER among the SNR range investigated. This verifies the accuracy of our Q-function approximation based analysis. Further, we can witness that the performance discrepancy between the simulated BER, ABEP-UB and ABEP-UPB minishes as  $A_T$  increases from 2 to 4. This can be explained as that the transmit spatial diversity achievable by the proposed system improves as  $A_T$  increases, which in turn, raises the accuracy of the approximate analysis of the ABEP performance. In addition, the BER performance is gradually deteriorating in all cases considered, as  $K$  increases from 1 to 5, and then to 10. This can be attributed to the presence of LoS and NLoS

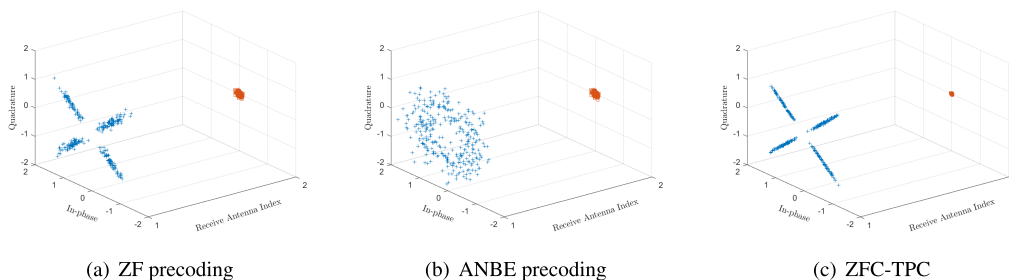


FIGURE 6. Three-dimensional constellation of receive signals achievable by the proposed RIS-PSM employing with different precoding schemes. SNR = -5 dB.

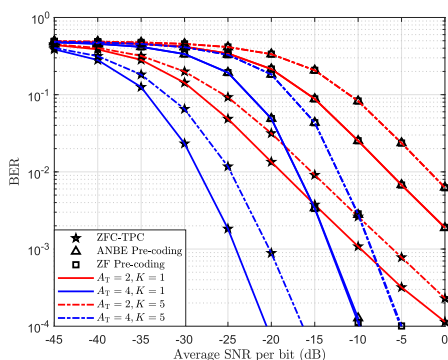


FIGURE 7. Comparison of BER performance achievable by the proposed RIS-PSM employing with different precoding schemes.

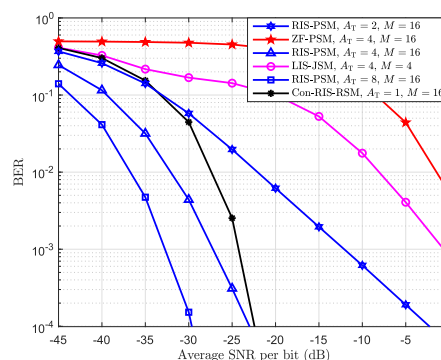


FIGURE 8. Comparison of the BER performance achievable by MIMO systems with specified configurations, which are modulated by different SDIM schemes.

components in the Rician fading channel. In the context of a PSM system considering Rician fading channels, an increase in the Rician factor  $K$  leads to a gradual amplification of the weight assigned to the LoS component, resulting in a general increase in the power of the LoS component while a decrease in that of the NLoS component decreases. Consequently, the fading process of the channel becomes more predominantly influenced by the LoS component, causing deterioration in the differentiation of channel between the transmitter and the RIS. This further leads to a degradation in the achievable spatial diversity gain, and hence makes it challenging for the receiver to effectively distinguish between signals for different antennas.

In Fig. 6, based on the comparison of the ZF precoding, alternative null-space beamforming (ANBE) precoding [37], and the proposed ZFC-TPC schemes, we illustrate the constellation dispersion observed at different receive antennas by taking the simulation of 200 times of channel realizations, and letting the selected receive antenna be specified as the first antenna. The blue cross mark denotes the signal constellations observed at the first receive antenna, while the red square mark represents the received signal constellations observed at the second receive antenna. By observing the constellations depicted in Fig. 6(c), we can explicitly achieve that the received signals of the specified receive antenna form a regular constellation pattern, while the constellations observed at the rest receive antenna is highly cohesive, indicating that the scheme has a certain degree of directivity

in signal reception at the designated antenna. In comparison, although the constellation pattern of the received signals at the specified receive antenna in Fig. 6(a), 6(b) can also form a regular pattern, there exists signal noises along with frequency deviations, which as a results, indicates negative effects on the receive quality of the RIS-PSM with ZF or ANBE precoding. On the hand, it further demonstrates the superiorities of our novel ZFC-TPC based RIS-PSM.

Fig. 7 compares the BER performance achievable upon employing the transmitter precoding schemes of ZF, ANBE, and our proposed ZFC-TPC, when the channel  $\mathbf{G}$  is supposed to obey Rician fading. From Fig. 7, we can observe that the BER performance obtained by utilizing the ZFC-TPC scheme is superior to that by the ZF or ANBE precoding scheme. This is due to that, in contrast to the other two precoding schemes, the ZFC-TPC scheme is designed by employing the Rayleigh-Ritz lemma, and can be utilized to completely eliminate the influence of the other antennas, as well as to make full use of the array elements of the introduced RIS to achieve a better BER performance. Moreover, the BER performance results of the ANBE and ZF schemes are gradually enhanced as  $A_S$  increases from 2 to 4, and that of the ZF, ANBE and ZFC-TPC schemes are getting worse gradually as  $K$  increases from 1 to 5. Additionally, we can also witness that, except for the ZFC-TPC scheme, there is little difference between the BER performance achievable by employing the other two precoding schemes.

Fig. 8 presents a fair comparison of the RIS-PSM, ZF-PSM [11], RIS-assisted RSM [18] (referred to as Con-RIS-RSM), and LIS-assisted joint transceiver SM (i.e. LIS-JSM) [19] with a given data rate of  $B = 5$  bits per channel utilization (bpcu). From the simulated results in Fig. 7, one can have that the BER performance of the proposed RIS-PSM scheme is generally better than that achievable by other SDIM counterparts. Specifically, the system BER performance of the Con-RIS-RSM would require at least a increase of 3 dB in SNR to achieve the same BER of  $10^{-3}$  as the RIS-PSM proposal in this paper. This is due to that, given the LIS-JSM is employed, the detection reliability can be degraded, as the detection of the activate transceive-antenna indices is simultaneously conducted. We can also observe from the figure that, the RIS-PSM system with  $A_T = 2$  achieves the worst BER performance among all the depicted cases. This is due to that, as  $A_T = 2$  and  $A_R = 2$ , the diversity gain of the system only provides by the multipath diversity gain of RIS and the diversity gain at the receiver. However, when  $A_T$  is increased from 2 to a larger number, there becomes the additional diversity gain output by the transmitter, which is substantiated for improving the system BER performance significantly. Moreover, in the Con-RIS-RSM scheme, the number of transmit antennas can only be 1, the system BER performance can not be enhanced by improving the transmit end spatial diversity. However, in the scenario of RIS-PSM assisted downlink, although the BER performance of RIS-PSM is worse than that of Con-RIS-RSM at  $A_T = 2$ , the system BER performance can be remarkable enhanced by continuous increasing the number of transmit antennas. From these perspectives, we can be convinced that, the proposed RIS-PSM is capable of trading the advantages engaged with the multipath spatial links between the transmitter and the RIS for remarkable enhancements in regard to both spatial diversity and error performance gains.

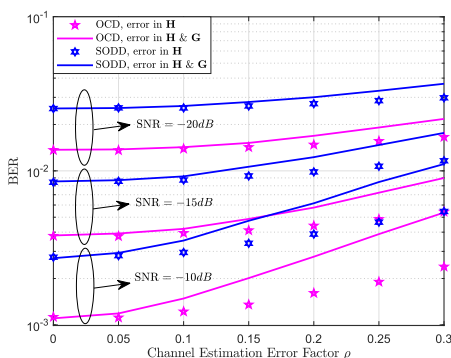


**FIGURE 9.** Comparison of the BER performance achievable by the proposed RIS-PSM with the detection of OCD and SODD under different channel conditions.

Fig. 9 demonstrates the impact of channel estimation with one-hop ( $\mathbf{H}$ ) or two-hop ( $\mathbf{H}\&\mathbf{G}$ ) errors on the BER performance of the OCD or SODD based RIS-PSM systems. Without loss of generality, the CSI achieved with imperfect

channel estimation of  $\mathbf{H}$  and  $\mathbf{G}$  can be modelled as  $\mathbf{L} = \sqrt{1 - \Delta^2} \hat{\mathbf{L}} + \Delta \tilde{\mathbf{L}}$ , where  $\mathbf{L} \in \{\mathbf{H}, \mathbf{G}\}$ ,  $\Delta \in [0, 1]$  represents the channel estimation error factor,  $\hat{\mathbf{L}}$  represents the channel estimation part (known part), while  $\tilde{\mathbf{L}}$  represents the channel estimation error (uncertain part). From Fig. 9, we can observe that the BER performance of the RIS-PSM system decreases with the increasing of  $\Delta$ . The BER performance of the RIS-PSM system with two-hop channel estimation error exhibits a higher performance loss than that with one-hop channel estimation error. Furthermore, under the same SNR conditions, the BER performance attainable by the OCD generally outperforms that by the SODD. Regardless of whether the OCD or SODD is employed, the BER performance achievable with low SNR is less affected by channel estimation errors than that in the high SNR region. This is due to the fact that an increase in channel estimation errors can cause a remarkable decrease in the receive SNR.

## VII. CONCLUSION

In this paper, we introduced and investigated a transmitter precoding framework enabled by RIS. Based on which, a non-convex problem of maximizing the output power of the specified receive antenna was formulated. We proposed the TPDP algorithm, which effectively optimizes both the transmitter precoding vector and the RIS reflecting coefficient matrix by detaching the non-convex problem into two sub-problems. To achieve the performance limit of receive detection, a high complexity OCD was initially designed, which was later proposed with a low complexity SODD implementation. Eventually, we evaluated the BER performance of the RIS-PSM system with OCD. Simulation results were depicted to demonstrate that the best error performance is achievable by the proposed ZFC-TPC based RIS-PSM, when compared with the ZF or ANBE precoding based RIS-PSM systems, the ZF-PSM, LIS-JSM, and the Con-RIS-RSM systems. Given the single case of ZFC-TPC based RIS-PSM, the error performance achieved by the SODD is comparable to that by the OCD algorithm with extensively decreased computational complexity. In summary, the proposed RIS-PSM is performance-superior and cost-effective to be implemented, and can be highly-flexible for facilitating the reliable transmission of RIS-assisted arbitrary-scale MIMO. In the future, we will consider a more complicated scenario where both direct link and RIS-involved indirect link coexist between the transmitter and receiver, while explore novel transmission techniques, so as to refine our research of RIS-PSM.

## REFERENCES

- [1] Y. Liu, X. Liu, X. Mu, T. Hou, J. Xu, M. Di Renzo, and N. Al-Dhahir, "Reconfigurable intelligent surfaces: Principles and opportunities," *IEEE Commun. Surveys Tuts.*, vol. 23, no. 3, pp. 1546–1577, 3rd Quart., 2021.
- [2] E. K. Hidir, E. Basar, and H. A. Cirpan, "On practical RIS-aided OFDM with index modulation," *IEEE Access*, vol. 11, pp. 13113–13120, 2023.
- [3] D. Demmer, F. F. Manzillo, S. Gharbieh, M. Smierchalski, R. D'Errico, J.-B. Doré, and A. Clemente, "Hybrid precoding applied to multi-beam transmitting reconfigurable intelligent surfaces (T-RIS)," *Electronics*, vol. 12, no. 5, p. 1162, Feb. 2023.

- [4] P. Wang, J. Fang, X. Yuan, Z. Chen, and H. Li, "Intelligent reflecting surface-assisted millimeter wave communications: Joint active and passive precoding design," *IEEE Trans. Veh. Technol.*, vol. 69, no. 12, pp. 14960–14973, Dec. 2020.
- [5] R. Y. Mesleh, H. Haas, S. Sinanovic, C. W. Ahn, and S. Yun, "Spatial modulation," *IEEE Trans. Veh. Technol.*, vol. 57, no. 4, pp. 2228–2241, Jul. 2008.
- [6] M. D. Renzo, H. Haas, A. Ghayeb, S. Sugiura, and L. Hanzo, "Spatial modulation for generalized MIMO: Challenges, opportunities, and implementation," *Proc. IEEE*, vol. 102, no. 1, pp. 56–103, Dec. 2014.
- [7] J. Jegannathan, A. Ghayeb, and L. Szczecinski, "Spatial modulation: Optimal detection and performance analysis," *IEEE Commun. Lett.*, vol. 12, no. 8, pp. 545–547, Aug. 2008.
- [8] C. Liu, L.-L. Yang, W. Wang, and F. Wang, "Joint transmitter–receiver spatial modulation," *IEEE Access*, vol. 6, pp. 6411–6423, 2018.
- [9] Y. Yang, Z. Bai, H. Liu, K. Pang, X. Hao, and K. J. Kim, "Design and performance analysis of spatial-index modulation based orthogonal time frequency space system," in *Proc. IEEE Int. Conf. Commun. Workshops (ICC Workshops)*, May 2022, pp. 922–927.
- [10] Q. Li, M. Wen, and M. Di Renzo, "Single-RF MIMO: From spatial modulation to metasurface-based modulation," *IEEE Wireless Commun.*, vol. 28, no. 4, pp. 88–95, Aug. 2021.
- [11] L.-L. Yang, "Transmitter preprocessing aided spatial modulation for multiple-input multiple-output systems," in *Proc. IEEE 73rd Veh. Technol. Conf. (VTC Spring)*, May 2011, pp. 1–5.
- [12] A. Abushattal and H. Arslan, "Phase index-based receive spatial modulation PHY security against supervised pattern recognition," in *Proc. IEEE Wireless Commun. Netw. Conf. (WCNC)*, Mar./Apr. 2021, pp. 1–5.
- [13] E. Faddoul, G. M. Kraidy, and I. Krikidis, "Low-complexity energy detection for spatial modulation," in *Proc. IEEE Global Commun. Conf. (GLOBECOM)*, Dec. 2022, pp. 6031–6036.
- [14] A. Mokh, M. Crussière, M. Hélar, and M. Di Renzo, "Theoretical performance of coherent and incoherent detection for zero-forcing receive antenna shift keying," *IEEE Access*, vol. 6, pp. 39907–39916, 2018.
- [15] A. A. Boulogeorgos and A. Alexiou, "Performance analysis of reconfigurable intelligent surface-assisted wireless systems and comparison with relaying," *IEEE Access*, vol. 8, pp. 94463–94483, 2020.
- [16] J. Yang, Y. Chen, M. Jian, J. Dou, and M. Fang, "Capacity improvement in reconfigurable intelligent surface assisted MIMO communications," *IEEE Access*, vol. 9, pp. 137460–137469, 2021.
- [17] J. Yao, J. Xu, W. Xu, C. Yuen, and X. You, "A universal framework of superimposed RIS-phase modulation for MISO communication," *IEEE Trans. Veh. Technol.*, vol. 72, no. 4, pp. 5413–5418, Apr. 2023.
- [18] E. Basar, "Reconfigurable intelligent surface-based index modulation: A new beyond MIMO paradigm for 6G," *IEEE Trans. Commun.*, vol. 68, no. 5, pp. 3187–3196, May 2020.
- [19] T. Ma, Y. Xiao, X. Lei, P. Yang, X. Lei, and O. A. Dobre, "Large intelligent surface assisted wireless communications with spatial modulation and antenna selection," *IEEE J. Sel. Areas Commun.*, vol. 38, no. 11, pp. 2562–2574, Nov. 2020.
- [20] J. Yuan, M. Wen, Q. Li, E. Basar, G. C. Alexandropoulos, and G. Chen, "Receive quadrature reflecting modulation for RIS-empowered wireless communications," *IEEE Trans. Veh. Technol.*, vol. 70, no. 5, pp. 5121–5125, May 2021.
- [21] K. S. Sanila and N. Rajamohan, "Intelligent reflecting surface assisted transceiver quadrature spatial modulation," *IEEE Commun. Lett.*, vol. 26, no. 7, pp. 1653–1657, Jul. 2022.
- [22] M. Wu, X. Lei, X. Zhou, Y. Xiao, X. Tang, and R. Q. Hu, "Reconfigurable intelligent surface assisted spatial modulation for symbiotic radio," *IEEE Trans. Veh. Technol.*, vol. 70, no. 12, pp. 12918–12931, Dec. 2021.
- [23] J. Ma, C. Liu, T.-X. Zheng, C. Liu, and G. Lu, "Augmented pattern index modulation empowered by RIS," in *Proc. IEEE Int. Conf. Commun. (ICC)*, May 2022, pp. 2858–2863.
- [24] R. Zhang, L.-L. Yang, and L. Hanzo, "Generalised pre-coding aided spatial modulation," *IEEE Trans. Wireless Commun.*, vol. 12, no. 11, pp. 5434–5443, Nov. 2013.
- [25] J. Luo, S. Wang, F. Wang, and W. Zhang, "Generalized precoding-aided spatial modulation via receive antenna transition," *IEEE Wireless Commun. Lett.*, vol. 8, no. 3, pp. 733–736, Jun. 2019.
- [26] C. Liu, L.-L. Yang, and W. Wang, "Transmitter-precoding-aided spatial modulation achieving both transmit and receive diversity," *IEEE Trans. Veh. Technol.*, vol. 67, no. 2, pp. 1375–1388, Feb. 2018.
- [27] K. S. Sanila and R. Neelakandan, "Enhanced precoding aided generalized spatial modulation for massive MIMO systems," in *Proc. Nat. Conf. Commun. (NCC)*, Jul. 2021, pp. 1–6.
- [28] K. S. Sanila and N. Rajamohan, "Joint spatial and reflecting modulation for active IRS assisted MIMO communications," *IEEE Trans. Commun.*, vol. 71, no. 5, pp. 3132–3143, May 2023.
- [29] X. Jin, X. Li, Z. Wu, and M. Wen, "RIS-aided joint transceiver space shift keying reflection modulation," *IEEE Commun. Lett.*, vol. 27, no. 3, pp. 891–895, Mar. 2023.
- [30] X. Zhang, *Matrix Analysis and Applications*. Cambridge, U.K.: Cambridge Univ. Press, 2017.
- [31] Z. Liu, C. Huang, Y. Yu, B. Fan, and J. Dong, "Fast attributed multiplex heterogeneous network embedding," in *Proc. 29th ACM Int. Conf. Inf. Knowl. Manage.*, Oct. 2020, pp. 995–1004.
- [32] V. Pugachev, *Probability Theory and Mathematical Statistics for Engineers*. Amsterdam, The Netherlands: Elsevier, 2014.
- [33] C. Liu, L.-L. Yang, and W. Wang, "Secure spatial modulation with a full-duplex receiver," *IEEE Wireless Commun. Lett.*, vol. 6, no. 6, pp. 838–841, Dec. 2017.
- [34] M. Simon and M. Alouini, *Digital Communications Over Fading Channels*. Hoboken, NJ, USA: Wiley, 2005.
- [35] M. Chiani, D. Dardari, and M. K. Simon, "New exponential bounds and approximations for the computation of error probability in fading channels," *IEEE Trans. Wireless Commun.*, vol. 24, no. 5, pp. 840–845, May 2003.
- [36] D. Tse and P. Viswanath, *Fundamentals of Wireless Communication*. Cambridge, U.K.: Cambridge Univ. Press, 2005.
- [37] C. Liu, J. Ma, P. Zhai, B. Liu, T.-X. Zheng, and F. Wang, "Enabling joint transmitter-receiver spatial modulation with RF mirrors: A low-cost and highly-flexible perspective," *Digit. Signal Process.*, vol. 133, pp. 1663–1683, Mar. 2023.



**CHAOWEN LIU** (Member, IEEE) received the B.S. degree in electrical engineering from the Henan University of Science and Technology, Luoyang, China, in 2011, and the Ph.D. degree in information and communication engineering from Xi'an Jiaotong University, Xi'an, China, in 2018. From 2015 to 2017, he was a Visiting Ph.D. Student with the School of Electronics and Computer Science, University of Southampton, U.K. He is currently a Lecturer with the Xi'an University of Posts and Telecommunications. His research interests include spatial-domain index modulation, physical-layer information security, full-duplex and metasurface-aided wireless, and covert communications.



**FEI YU** received the B.S. degree from Luoyang Normal University, Luoyang, China, in 2021. He is currently pursuing the M.S. degree with the Xi'an University of Posts and Telecommunications, Xi'an, China. His research interests include physical layer security, intelligent reflecting surfaces, and covert communications.



**ZHENGMIN SHI** (Graduate Student Member, IEEE) received the B.S. degree from the Xi'an University of Posts and Telecommunications, Xi'an, China, in 2022, where he is currently pursuing the M.S. degree in electronic and information engineering. His research interests include spatial modulation, intelligent reflecting surfaces, and physical layer security.



**MENGHAN LIN** (Graduate Student Member, IEEE) received the B.E. degree in information engineering from Xi'an Jiaotong University, Xi'an, China, in 2018, where he is currently pursuing the Ph.D. degree in information and communication engineering. His research interests include covert communication and source location privacy.



**FASONG WANG** received the B.S. and M.S. degrees in applied mathematics from the China University of Geosciences, China, in 2002 and 2005, respectively, and the Ph.D. degree in communication engineering from Xidian University, in 2013. He was a Senior Engineer with the 27th Research Institute, China Electronics Technology Group Corporation, Zhengzhou, Henan, China, until 2010. From 2016 to 2017, he was a Visiting Scholar with the Southampton Wireless Group, University of Southampton. He is currently a Professor with the School of Electrical and Information Engineering, Zhengzhou University, China. His current research interests include wireless communications, blind signal processing, sparse representation, machine learning, and their applications. He has published more than 40 journal and conference papers on these topics.



**CHENXI PANG** received the B.S. degree from the Xi'an University of Posts and Telecommunications, Xi'an, China, in 2022, where he is currently pursuing the M.S. degree in information and communication engineering. His research interests include spatial modulation, intelligent reflecting surfaces, and signal and information processing.



**JIANKANG ZHANG** (Senior Member, IEEE) is currently a Senior Lecturer with Bournemouth University. Prior to joining Bournemouth University, he was a Senior Research Fellow with the University of Southampton, U.K. He was a Lecturer, from 2012 to 2013, and then an Associate Professor, from 2013 to 2014, with Zhengzhou University. His research interests include aeronautical communications and networks, evolutionary algorithms, machine learning algorithms, and edge computing. He serves as an Associate Editor for IEEE Access.

...